HHS Public Access

Author manuscript

*ACS Appl Polym Mater*. Author manuscript; available in PMC 2021 April 07.

Published in final edited form as:

*ACS Appl Polym Mater*. 2020 March 13; 2(3): 1134–1144. doi:10.1021/acsapm.9b00921.

# Antimicrobial Peptide–Polymer Conjugates for Dentistry

**Sheng-Xue Xie**,
University of Kansas (KU), Lawrence, Kansas

**Linyong Song**,
University of Kansas (KU), Lawrence, Kansas

**Esra Yuca**,
University of Kansas (KU), Lawrence, Kansas, and Yildiz Technical University, Istanbul, Turkey

**Kyle Boone**,
University of Kansas (KU), Lawrence, Kansas

**Rizacan Sarikaya**,
University of Kansas (KU), Lawrence, Kansas

**Sarah Kay VanOosten**,
University of Kansas (KU), Lawrence, Kansas

**Anil Misra**,
University of Kansas (KU), Lawrence, Kansas

**Qiang Ye**,
University of Kansas (KU), Lawrence, Kansas

**Paulette Spencer**,
University of Kansas (KU), Lawrence, Kansas

**Candan Tamerler**
University of Kansas (KU), Lawrence, Kansas

## Abstract

Bacterial adhesion and growth at the composite/adhesive/tooth interface remain the primary cause of dental composite restoration failure. Early colonizers, including *Streptococcus mutans*, play a critical role in the formation of dental caries by creating an environment that reduces the adhesive's integrity. Subsequently, other bacterial species, biofilm formation, and lactic acid from *S. mutans* demineralize the adjoining tooth. Because of their broad spectrum of antibacterial activity and low risk for antibiotic resistance, antimicrobial peptides (AMPs) have received

**Corresponding Author**: ctamerler@ku.edu. Complete contact information is available at: https://pubs.acs.org/10.1021/acsapm.9b00921.

Supporting Information

The Supporting Information is available free of charge at https://pubs.acs.org/doi/10.1021/acsapm.9b00921.

Molecular structure of the AMPs and MA-AMPs confirmed by using FTIR, real-time conversion of C═C bond of the control and experimental adhesives, water sorption of the control group as a function of soaking time; representative stress–strain curves from compression test on PolyHEMA (hydrogel analogue), 0-5, and C0-10 cylindrical samples (PDF)

The authors declare no competing financial interest.

significant attention to prevent bacterial biofilms. Harnessing the potential of AMPs is still very limited in dentistry—a few studies have explored peptide-enabled antimicrobial adhesive copolymer systems using mainly nonspecific adsorption. In the current investigation, to avoid limitations from nonspecific adsorption and to prevent potential peptide leakage out of the resin, we conjugated an AMP with a commonly used monomer for dental adhesive formulation. To tailor the flexibility between the peptide and the resin material, we designed two different spacer domains. The spacer-integrated antimicrobial peptides were conjugated to methacrylate (MA), and the resulting MA–AMP monomers were next copolymerized into dental adhesives as AMP–polymer conjugates. The resulting bioactivity of the polymethacrylate-based AMP conjugated matrix activity was investigated. The antimicrobial peptide conjugated to the resin matrix demonstrated significant antimicrobial activity against *S. mutans*. Secondary structure analyses of conjugated peptides were applied to understand the activity differential. When mechanical properties of the adhesive system were investigated with respect to AMP and cross-linking concentration, resulting AMP–polymer conjugates maintained higher compressive moduli compared to hydrogel analogues including polyHEMA. Overall, our result provides a robust approach to develop a fine-tuned bioenabled peptide adhesive system with improved mechanical properties and antimicrobial activity. The results of this study represent a critical step toward the development of peptide-conjugated dentin adhesives for treatment of secondary caries and the enhanced durability of dental composite restorations.

## Graphical Abstract

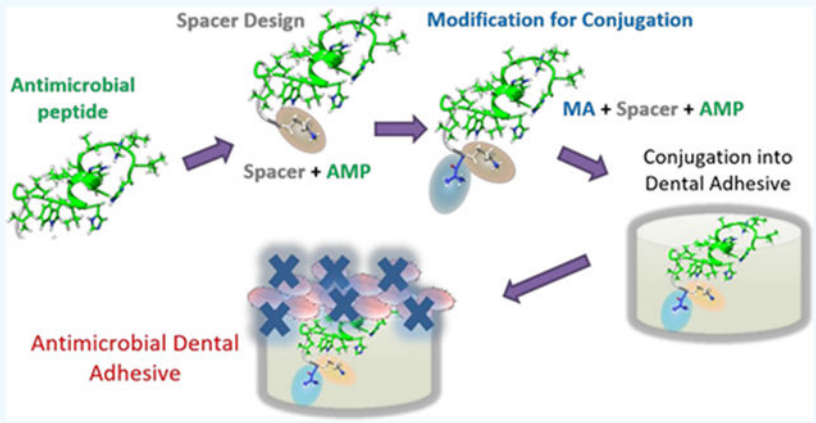


### Keywords

bioconjugation; antimicrobial peptide; dental adhesive; Streptococcus mutans; mechanical property; bioactivity

## INTRODUCTION

Despite the increased use of resin-based dental adhesive/composites in restorative dentistry,[1,2] these posterior composite restorations lack the sustained durability associated with classic dental amalgams.[3,4] Composite restorations fail twice to three-and-a-half times more frequently than amalgam due to secondary decay resulting from local bacterial infiltration.

[5–8] Bacterial adhesion and growth permeates to the adhesive/dentin interface between composite material and tooth, resulting in an ineffective seal.[6,9] *Streptococcus mutans* (*S. mutans*) is a Gram-positive, facultative anaerobic microorganism that has been implicated as the primary causative agent in the formation of dental caries.[10,11] Adhesion of *S. mutans* to the adhesive/dentin interface creates an environment that supports the subsequent attachment and growth of other bacterial species, ultimately leading to a microecosystem known as a biofilm. In addition to its role as a "pioneer" organism in biofilm formation, *S. mutans* produces lactic acid, which has been shown to damage the adjacent tooth surface permanently through demineralization.[12] The composite restoration's interface with the tooth degrades more rapidly than the interface formed by amalgam as bacterial biofilms and active enzymes thrive and permeate into the adhesive/dentin (a/d) interfacial defects and destroy the adjacent tooth structure.[13]

Numerous studies have investigated a variety of techniques to prevent *S. mutans* colonization by incorporating moieties such as fluoride-releasing compounds,[14] silver nanoparticles,[15,16] zwitterionic components,[16,17] and quaternary ammonium compounds (QACs).[15,18] Because of the release of small molecules by QACs and the rising concern on their contribution to antibiotic resistance,[19,20] a critical focus has been shifted toward developing alternative approaches to reduce or inhibit the biofilm formation at the adhesive/dentin interfaces. None of these techniques match the need for a broad-spectrum antimicrobial substance that prevents bacterial colonization at the fragile a/d interface, minimizes bacterial resistance while displaying long-term stability, and has a low cytotoxicity profile. Recently, antimicrobial peptides (AMPs) have received significant attention as a viable biomolecular alternative due to their superior bacteria killing characteristics and broad-spectrum activity. The AMPs are part of the innate immune response found in wide variety of life forms.[21–25] In recent years, AMPs have been shown in dental applications as coating agents for implants[26,27] or formulation additives for adhesive materials[28,29] to combat pathogenic microorganisms.[30] However, successful commercial applications that harness the vast potential of AMPs are still very limited in dentistry. This is partially due to their systematic distribution which mostly require high concentration raising concerns regarding potential toxicity.

In tissue engineering[31,32] or surgical wound dressings,[33–35] peptides have been successfully incorporated into hydrogels via conjugation. Several groups including ours studied to integrate antimicrobial peptide to polymer systems.[31,36–40] Because of AMPs' rapid and complete clearance and the toxicity risk that is associated with using high systemic concentrations, many groups have explored different conjugation strategies to design AMP–polymer conjugates. Kumar et al.[38] demonstrated useful AMP activities after conjugation to hyperbranched polyglycerol. Depending on the requirement of the composite materials dictated by the application area, these approaches also offer promising drug delivery systems. Studies have explored the interdependent relationship of these conjugates by optimizing their biologic functionalities through tuning the physical properties.[41–43] Despite successful antimicrobial efficacy, current development of natural or synthetic hydrogels featuring AMPs or antibiotic substances indicated that the resulting material had low mechanical strength. This could be a concern for durability in particular in load-bearing applications, such as in dentistry. The typical compression moduli of AMP-hydrogel

conjugates varied from about 0.1 to ~40 kPa,[31,36,44–49] which is less than ideal for use in dental restorations. The reported Young's modulus of hydrated commercial dental adhesives ranged from 0.5 to 4 GPa at 37 °C,[50,51] which were mainly affected by the chemical composition and temperature. Meanwhile, addressing the lack of mechanical strength of the polymer matrix through cross-linker concentration while retaining antimicrobial efficacy of AMPs has not yet been shown.[46]

Dental materials capable of antimicrobial activity have previously been developed by introducing polymerizable quaternary ammonium salts (QAC), such as methacryloyl-oxydodecylpyridinium bromide (MDPB).[52,53] However, their efficacy to reduce oral bacteria has not been fully elucidated. While co- and cross-resistance to various of antibiotics have been linked to QAC resistance, their efficacy to reduce oral bacteria has not been fully elucidated. To overcome these challenges, there are several alternative approaches explored in the literature.[54,55] AMPs have potential advantages because of unique mechanisms of action, rapid activity, and ability as host defense functions as innovative therapeutic antimicrobial agents. Their high concentration for effective dosage, sensitivity to ion strength, and potential immunogenicity have limited their usage.[56]

In a recent study, nisin, an established antimicrobial peptide, was loaded into Single Bond 2, a commercially available adhesive using nonspecific adsorption.[57,58] Cured nisin-incorporated dental adhesive exhibited an inhibitory effect against *S. mutans* growth. The antimicrobial efficacy increased with increasing nisin concentrations. However, no significant differences were noted in the agar diffusion test for the cured nisin-incorporated adhesives when compared to control formulations.[57,58] The result indicates that the antibacterial effect by inclusion of nisin occurs within the adhesive. Previously, we have also demonstrated the efficacy of a modified version of the established antimicrobial peptide GH12,[59–61] GH12-M2 (GLLWHLLHHLLH_GSGGG_K), against *S. mutans* using nonspecific adsorption.[29] Moussa et al. have demonstrated a two-tier strategy—hydrophobic and antibiofilm protection scheme—for adhesive-based interfaces by using amphipathic and antimicrobial peptides to obtain hydrophobic and antibacterial dentin that resists recurrent caries around bonded restorations.[62,63] They applied a priming strategy for dentin coating, which offers a promising technology. It would be interesting to address the depth of the penetration of the adhesive into the dentin.

Nonspecific interactions of AMPs with polymers may limit the peptides' availability, causing reduced antibacterial efficacy. To overcome the challenge of the peptide leaking from the resin due to nonspecific adsorption as well as limiting active conformations, this study aims to incorporate a tunable AMP sequence specifically conjugated to a commonly used monomer for dental adhesive formulation. As conjugation of the AMP may also pose efficacy challenges due to the limiting optimum conformation, we designed a spacer domain to allow flexibility between the peptide and the resin material. In addition to providing an orientation control for the peptides, the spacer domain offers a method for both retaining the ability to conjugate to the polymer while providing a distance away from the conjugated polymer to display the peptide. Several novel, AMP monomers were first synthesized using GH12 derivative sequences to enable subsequent methacrylate conjugation. A 12-amino acid peptide GH12 with optimal structure and potency against *S. mutans*[59,60] was selected as an

AMP for further sequence modifications. The resulting bioactivity was investigated as the AMP monomers were polymerized into the polymethacrylate-based matrix activity. We performed secondary structure analyses to relate the effect of spacer on activity by studying features that can be highly relevant for antimicrobial activity.[64–66] Biomolecular characterization and functional activity of our engineered dental adhesive formulations were assessed. The antimicrobial peptide conjugated to the resin material (MA-AMP) demonstrated significant antimicrobial activity against *S. mutans*. We next investigated the mechanical properties. Peptides bearing polymerizable C═C bonds are synthesized by using Fmoc chemistry to be readily anchored onto dental adhesive polymer via free radical polymerization. A peptide conjugated with methacrylic acid (MA) is referred as a peptide monomer bearing polymerizable C═C bonds originating from MA. Such a design approach can be used with different monomers, oligomers, and polymers. These peptide monomer to oligomer combinations allow the system to be applicable to wide range of combinations prior to polymerization reactions. Our antimicrobial peptide-adhesive hybrid system design offers a promising approach for advancing the integration of biofunctional properties into the polymeric materials design to address different challenges targeting tissue engineering applications as well as providing therapeutic approaches at hybrid interfaces.

## EXPERIMENTAL SECTION

### Materials.

Triethylene glycol dimethacrylate (TEGDMA), 2-hydroxyethyl methacrylate (HEMA), 2-methacryloyloxyethyl-phosphorylcholine (MPC), methacrylic acid (MA), camphoroquinone (CQ), ethyl 4-(dimethylamino)benzoate (EDMAB), diphenyliodonium hexafluorophosphate (DPIHP), dodecyltrichlorosilane, chlorhexidine digluconate (CHX), *N,N*-dimethylformamide (DMF), dichloromethane (DCM), and *N*-methylmorpholine (NMM) were obtained from Sigma-Aldrich (St. Louis, MO) and were used as received without further purification. Piperidine and alamarBlue Reagent were obtained from Fisher. Rink amide resin, Fmoc-amino acid building blocks, and 2-(1*H*-benzotriazole-1-yl)-1,1,3,3-tetramethyluranium hexafluorophosphate (HBTU) were purchased from AAPPTec LLC. BD Bacto brain heart infusion, BD BBL dehydrated brain heart infusion agar, and Corning Clear polystyrene 96-well microplates (Corning 3370) were obtained from Fisher. *S. mutans* UA159 bacterial strain was from American Type Culture Collection (ATCC 700610). Methacrylated AMP monomers (MA-AMP) were synthesized within our laboratory.

### Synthesis of MA-Peptide Monomers.

MA-peptide monomers, including MA-AMP and MA-non-AMP (non-antimicrobial active peptide control) monomers were synthesized via an amidation reaction between the free amine group (peptide) and carboxylic acid group (MA). Briefly, Fmoc-resin-bound peptide with a spacer was first synthesized through Fmoc chemistry by using a solid-phase peptide synthesizer (AAPPTEC Focus XC). Upon peptide-chain completion (including spacer sequence), methacrylic acid, NMM, and HBTU were added to react with the Fmoc-resin-bound peptide in DMF at 23 ± 2 °C overnight under constant gentle rotation. After the conjugation reaction, the Fmoc-resin-bound product was washed sequentially with DMF, DCM, acetone, and ethanol. The crude MA-peptide monomer was then cleaved from the

Fmoc-resin and purified on a HPLC system (Waters Corp., Milford, MA) equipped with a Luna column packed with 10 μm C18 silica (250 × 10 mm, Phenomenex Inc., Torrance, CA). The pure MA-peptide monomer was lyophilized, and powder was subsequently stored in a freezer at −20 °C. The correct molecular weight of each MA-peptide monomer was confirmed by electrospray ionization mass spectrometry using a Qtof Premier (Waters Corp., Milford, MA) instrument.[67] The MA-peptide monomer solution was prepared from fresh stock peptide powder for every experiment.

### Preparation of Adhesive Formulations.

Formulations without MA-AMP were used as the polymer-only controls. The experimental formulation contained 10 wt % of MA-AMP monomers. The resin mixtures were prepared in an amber glass vial and mixed for 2 h at 23 ± 2 °C to ensure complete dissolution and promote the formation of a homogeneous solution. Detailed polymer formulations and components are shown in Table S1 as wt %.

### Preparation of Polymer Samples.

Round discs (4 mm diameter and 1.2 mm thickness) and cylindrical polymer specimens (5 mm diameter and 1.7 mm thickness) were used to perform antimicrobial activity tests and mechanical compression tests, respectively. The prepared resins were injected into a Tzero Hermetic Lid (P/N: 900797.901) or Tzero low mass pan (P/N: 901683.901), covered with a dodecyltrichlorosilane-modified glass cover (22 mm × 30 mm, Fisherfinest), and then light-cured for 40 s at 23 ± 2 °C by using a commercial visible light lamp (Spectrum 800, Dentsply, Milford, DE, intensity = 550 mW/cm$^2$). The polymerized samples were stored in the dark at 23 ± 2 °C for at least 48 h before testing.

### Streptococcus mutans Culture.

The antimicrobial efficacy of control formulations, AMPs only, and MA-AMP monomers was assessed by using an *S. mutans* UA159 bacterial strain model (American Type Culture Collection (ATCC 700610). Following ATCC standard protocol, the lyophilized bacteria were reconstituted in BHI medium (BD Difco) and streaked onto a prepared BHI agar plate (BD Difco). The stock culture plate was incubated for 24 h at 37 °C with 5% carbon dioxide ($CO_2$). Overnight cultures of *S. mutans* UA159 were prepared fresh, prior to each experiment, by inoculating 10 mL of fresh BHI medium with a single colony selected from the stock culture plate and incubated for 16 h. The overnight cultures were diluted in fresh BHI media and growth was monitored via optical density measurements at 600 nm (OD600) on a Cytation3 multimodal plate reader (BioTek).[69]

### Antimicrobial Activity of Peptide and MA-Peptide Monomer.

Inhibitory concentration assays were conducted by using a standard broth microdilution method, according to Clinical and Laboratory Standards Institute (CLSI) protocol.[70,71] Briefly, 2-fold serial dilutions of compounds were prepared with sterile deionized water to achieve concentrations ranging from 5 to 1250 μg/mL in a volume of 20 μL, after which 80 μL of BHI broth and 100 μL of bacterial culture containing 2 × 10$^4$ CFU/mL were added. Thus, each well contained peptide or MA-peptide monomer concentrations ranging from 0.5

to 125 μg/mL and a final bacterial concentration of $1 \times 10^4$ CFU/mL. The well that exclusively contained *S. mutans* served as the negative control for bacterial growth/negative control for antibacterial activity. The positive control for bacterial growth/positive control for antibacterial activity was identical to the negative control, except that the 20 μL $H_2O$ was replaced with 20 μL of 63 μg/mL CHX solution. The blank well contained 20 μL of $H_2O$ and 180 μL of medium without cells. The 96-well plate was incubated in the presence of 5% $CO_2$ at 37 °C overnight. The solution of each well was transferred to a new plate. The bacterial cell viability was assessed by fluorescence intensity by using an established alamarBlue assay.[72,73] The minimum inhibitory concentration (MIC) value was defined as the lowest peptide or MA-peptide monomer concentration corresponding to the zero-value measured via alamarBlue assay. Experiments were repeated a minimum of three times per specimen treatment and concentration.

### Antimicrobial Activity Assays of Resin-Disc Diffusion in Solution.

In-solution antimicrobial activity of peptide conjugated resin discs was assessed. The round disc polymer specimens were soaked in water for 5 days to remove the unreacted components[74] and were subsequently assessed for in-solution antimicrobial activity. Briefly, the soaked disc samples were blotted to remove excess water on the surface, and one disc was transferred to the microwell in a 96-well plate. Next, 20 μL of $H_2O$, 80 μL of BHI broth, and 100 μL of BHI broth containing $2 \times 10^4$ CFU/mL *S. mutans* cells were added to each well to a final bacterial concentration of $1 \times 10^4$ CFU/mL. After incubation in the presence of 5% $CO_2$ at 37 °C overnight, the solution of each well was transferred to a new plate and alamarBlue dye was added, following the manufacturer's protocol. Samples were incubated for 2 h before fluorescence intensity was measured at Ex565/Em595. The well that only contained *S. mutans* served as the negative control. Polymer-only demonstrates the antibacterial activity of the system without MA-peptide monomer in the formulation. Peptide control was a disc made from MA-non-AMP with GGG as a spacer. NonAMP was a peptide without antimicrobial activity. This specimen treatment demonstrates the antibacterial activity of the system with a MA-peptide monomer in which the peptide is known to have undetected antibacterial activity alone in solution. The positive control for growth was identical to the negative control, except that the 20 μL of $H_2O$ was replaced with 20 μL of 63 μg/mL CHX solution. The blank well contained 20 μL of $H_2O$ and 180 μL of medium without cells. Experiments were repeated a minimum of three times per specimen treatment.

### Compression Test.

The mechanical properties of formulations that are composed of peptides with either 5% w/w cross-linker (polymer-only-5) or 10% w/w cross-linker (polymer-only-10) amounts were measured by a compression test on a Deben Microtest compression stage (Microtest 2kN Stage, Deben UK Ltd., Bury St Edmunds, UK) at 23 ± 2 °C. The hydrated cylindrical samples were obtained by soaking the sample in water for 5 days. After the diameter and thickness of the hydrated sample were measured from images by using Adobe Photoshop 7.0 software (Adobe Systems Incorporated, San Jose, CA), it was placed on the lower plate of the compression stage and compressed at a loading rate of 2 mm/min. The diameter and thickness of the hydrated samples are 6.57 ± 0.06 mm (C0-5), 2.28 ± 0.06 mm (C0-5), 6.14

± 0.08 mm (polymer-only-10), and 2.10 ± 0.08 mm (polymer-only-10). The force and displacement were recorded by using Deben Microtest software (Version 5.4.3) with a sampling time 0.1 s. The Young's modulus, defined as the slope of the linear region of the stress–strain profile, was calculated from the initial linear region of the curve (<15% strain). Nine specimens of each formulations were analyzed.

### Computational Peptide Flexibility and Structure Feature Prediction.

Multiple batches of 1000 structures were generated in PDB file format by a custom PyRosetta peptide folding script used previously.[29] The PyRosetta folding script is a fragment-insertion based method using fragments from the Robetta server.[75] Each structure is an independent optimization which shares the fragment database with the other structures of the same sequence. DSSP software[76] was used to calculate the flexibility and structure features on each structure generated. The flexibility and structure-feature frequency variation between batches was calculated as the coefficient of variation (CV). The numerator s is the sample standard deviation of the mean of each batch, and $x$ is the sample mean of all batches.

$$\mathrm{CV} = \frac{s}{x} \tag{1}$$

Using computational approaches, we explored whether there are certain structural features relevant to experimentally measured activity. We next examined the bond patterns and bending orientation between residue chains using a widely used fragment insertion method to fold peptides. The names and abbreviations in our analysis refer to the features that are defined by the Dictionary of Secondary Structure of Protein (DSSP) program, a widely used program for labeling secondary structures in proteins.[76] The "Turn" refers to if there is a hydrogen bond from the residue's carbonyl to an adjacent residue's amide. A "Bend" is a dihedral angle magnitude of more than 70°. The "LH-RH" refers to the chirality of the dihedral angle, with "LH" referring to a positive, left-handed rotation and "RH" referring to a negative, right-handed rotation.

The "3-10" and "$\alpha$" are for secondary structure helix types occurring at a specific residue. The colored pie is a representation of the position of the side chains. If two residues are part of the same helix and the colored pies overlap, then the residue side chains are in the same helical face, like neighboring helical positions in a wheel plot.

The grayscale coloring system conveys both the magnitude of the frequency of a feature at a specific residue position and its variability; i.e., a frequency of 100% is black, and a frequency of 0% is white. As Rosetta generation is stochastic, multiple ensembles of 1000 structures will vary. Therefore, we generate three ensembles of 1000 structures to measure the variability between ensembles. The magnitude of the frequency is the arithmetic mean of the frequency across ensembles. This is the grayscale level of the central icon for the frequency. The variability of the frequency is the coefficient of variation (CV), standard deviation of the frequency across ensembles divided by the mean frequency across the ensembles. This is the border grayscale for the frequency icon. For frequencies in which the

mean is much greater than the CV, the frequency image is a dark icon with a white or light gray border. For a frequency feature with a large CV and a small mean value, the image is a light icon with a dark gray border.

### Statistical Analyses.

For all experimental groups, the differences were evaluated by using one-way analysis of variance (ANOVA), together with Tukey's test at $\alpha = 0.05$ to identify significant differences (OriginPro Version 8.0, OriginLab Corporation, North-ampton, MA

## RESULTS AND DISCUSSION

Herein, we engineered and synthesized several MA-peptide monomers consisting of a methacrylic acid linked to either a non-AMP peptide (control formulation) or to an AMP (GH12-derived peptide)[59–61] with different oligomeric spacers.[65,66,77] The N-terminal lysine (K) in each spacer provides the reactive amino group for MA functionalization.

### Antibacterial Activity.

We examined the effects of two different spacers to improve antimicrobial activity. The sequences, conjugation sites, and the Inhibitory concentration ($IC_{50}$) and MIC values of designed AMPs, MA-non-AMP, and MA-AMP-monomers are provided in Table 1. The $IC_{50}$ value was defined as the lowest peptide concentration corresponding to 50% inhibition of cellular viability measured via the alamarBlue assay. MIC values of AMPM3 and AMPM5, MA-AMPM3, and MA-AMPM5 were calculated at 7.8, 15.6, 7.8, and 15.6 $\mu$g/mL, respectively. After the introduction of the C═C bond originating from MA onto the AMPs, MIC values of MA-AMPM3 and MA-AMPM5 were not affected as compared to AMPM3 and AMPM5, respectively. IC50 values of AMPM3 and AMPM5, MA-AMPM3, and MA-AMPM5 showed a similar pattern (Table 1 and Figure 1).

Both MA-AMPM3 and MA-AMPM5 were amidated at the C-terminus, such that MA-AMPM3 corresponded to the spacer GGG[66] and MA-AMPM5 to the spacer SSSGGG,[77] The results indicate that the MA-AMPM3 monomer had the lowest MIC value which corresponds to the highest antimicrobial activity as compared to the sequences featuring the M5 spacer.

Next, we studied the antimicrobial activity of AMP-polymer conjugates incorporated into polymerized discs against *S. mutans.* At low cross-linker concentration, both peptide control-5 (polymer conjugates with 5% cross-linker and MA-non-AMP) and polymer-only-5 (polymer conjugates with 5% cross-linker) control did not show inhibition against *S. mutans* bacterial growth (Figure 2). MA-AMPM3–5 (polymer conjugates with 5% cross-linker and MA-AMPM3), however, exhibited substantial antimicrobial activity. As shown in Figure 2, it was noted that MA-AMPM5–5 (polymer conjugates with 5% cross-linker and MA-AMPM5) did not display significant inhibition against *S. mutans*. MA-AMPM3 with GGG spacer significantly improved antimicrobial activity as compared to MA-AMPM5 with the SSSGGG spacer in the cross-linked conjugates. The GGG spacer as a linker is markedly better than the SSSGGG spacer for antimicrobial activity in the polymerized material. The MIC values of MA-AMPM3 and MA-AMPM5 in the monomeric state were observed not to

be significantly different; we therefore performed the antimicrobial activity tests on both samples (Table 1). However, the polymerized samples that are the conjugated with the MA-AMPM3 having GGG spacer demonstrated a better antimicrobial activity as compared to MA-AMPM5 designed with the SSSGGG spacer. The improved antimicrobial activity following polymerization associated with the GGG spacer may be attributed to the conformational differences of the secondary structure of the active antimicrobial peptide.

### Effect of the Spacer Sequence on the Structural Flexibility.

The effect of the spacer sequence on the structural flexibility and feature frequency of the GH12 peptide was evaluated through statistical analyses performed on the batches of structures computationally generated by using a fragment-insertion technique. For AMPM3, the spacer sequence is GGG, and for AMPM5 the sequence is SSSGGG. The domain of GH12 was also analyzed separately. While the longer spacer reduced the antibacterial activity of the GH12 domain, the AMPM5 still shows statistically significant antibacterial activity.

In a recently published paper, our group studied the structure of GH12 and a modified GH12 with a spacer through CD signal analysis and PyRosetta structure generation.[29] This study provided evidence that adding a spacer to the GH12 peptide did not significantly affect the peptide's folding in-solution. The structural analysis of both methods concluded that the addition of the spacer did not affect the peptide structure ensemble. The activities of the GH12 and the modified version were evaluated by soaking the peptide in the polymer solution, demonstrating that the polymer environment did not inactivate the GH12 activity with the spacer. The previous study's results were followed by conjugating two spacer-GH12 peptide variants to evaluate the activity of the resulting hybrid peptide–polymer materials. Figure 2 of this study shows a strong effect of the spacer selected on the activity of the GH12 when conjugated in the material and a minor effect on the activity of the GH12 domain in-solution. A slight change in the MIC is shown between peptides with the same antimicrobial peptide domain and different spacers (Table 1). The change in activity of the conjugated versions GH12 cannot be adequately explained by only considering the in-solution MIC results. Therefore, we investigated how the spacer plays a role in changing the folding of active peptide domains when integrated into polymeric materials. Obtaining a CD signal of the insoluble hybrid peptide–polymer material requires specialized techniques to overcome the solvent shift effect and differential light scattering identified when including hydrophobic phases in solutions for CD analysis, such as for cellular membranes when studying membrane proteins.[78] Describing spacer-related differences to active domains is of high interest to the field of hybrid polypeptide/polymer systems. Therefore, we used the PyRosetta tools to investigate what change in structure trends the spacer may be involved in. While the Rosetta-generated structures lack the explicit modeling of the conjugation with the polymer, the method provides the most accurate simulation of large ensembles of peptide structures to estimate folding dynamics the authors are aware of while avoiding the computational cost of using molecular dynamics simulations.

Although the length and rigidity have been shown to be important features of designing spacers in chimeric peptides and proteins[67,79,80] of antibacterial functionality, the length and

rigidity of the compared spacers do not appear to be positively related to retained conjugation activity in this study of antibacterial functionality. From previous studies, an increase in spacer length has been shown to result in increased antibacterial activity. This relationship was not seen in this study. A short spacer of four residues resulted in improved retention of conjugated activity compared to a six-residue spacer that shares the same N-terminal residue a three-residue motif with the shorter spacer. The additional SSS residues in AMPM5 show hydrogen-bonding patterns at S3 and S4 which are at the darkest grayscale for the turn feature among any of the residues in the three panels of Figure 3. These hydrogen bonds increase the rigidity of the backbone of the spacer domain compared to the KGGG spacer with less estimated hydrogen bonds as seen by a lighter grayscale at AMPM3-GGG compared to AMPM5-SSS. While the frequency of hydrogen bonding is relatively high in the AMPM5-SSS region, the hydrogen bonds are less likely to result in helical formations. The $\alpha$ helix formation rate is below the detection limit of the stochastic generation method used. The $3_{10}$-helix formation rate is above the detection limit, but it is below the observed formation rate in the top panel LWH region despite the turn frequency in at GH12-W4 being smaller than the turn frequency at AMPM5-S3.

While the foldings of the GH12 domain in the bottom two panels of Figure 3 are similar to one another, the GH12 domain is different than the top panel with no spacer. These secondary structure frequency differences provide design targets for spacers to aid in the retention of conjugated polypeptide activity. Understanding the folding effect of spacers by modeling the full sequence with the spacer will greatly enhance the success of designed spacers to retain that activity of polypeptides that are conjugated to polymeric materials.

The folding of AMPM3 shares more similarity to GH12 than the folding of AMPM5. The variability of the turn prediction is darker for AMPM5 than for AMPM3 or for GH12. The $3_{10}$-helix feature trend is roughly the same for AMPM3 and AMPM5, predicting five of the $3_{10}$-helix residues, but different than GH12, which predicts nine of the $3_{10}$-helix residues. GH12 also predicts six of those nine residues to be involved in $\alpha$-helix occurrence. These structure feature patterns may be recovered in modified peptides through future spacer designs which conserve the $\alpha$-helix occurrence. These modified peptides will enable understanding if this feature specifically leads to improved antibacterial activity.

As a final comparison of the structural features of the modified peptides studied and the GH12 domain alone, the LH-RH feature tracks if the peptide backbone twists to the left or to the right between residues. This feature is a consistent change between batches of structures of AMPM3 and AMPM5. AMPM5 has more right-handed twists of the peptide backbone for the last three residues than AMPM3. The trend of twists for GH12 for the final five residues matches the trend of AMPM3 and not AMPM5. This trend relates to the relative orientation of side chains to each other in the antibacterial domain sequence. Having these orientations be more conserved by using the GGG spacer instead of the SSSGGG spacer seems to have led to conserved antibacterial activity of the GH12 domain.

In addition to the flexibility analysis discussed previously, multiple factors may influence the antimicrobial function of the conjugated peptides.[26] A bifurcated hydrogen bonding might be produced between a polar serine $\gamma$ oxygen and the NH of other residues in the main

chain. The interactions between the specific side chain and the main chain could destabilize in-solution secondary $\alpha$-helical structures of the AMP in comparison to the spacer (GGG).[80] Parameters such as composition and the structural flexibility/rigidity of the spacer, surface concentration, and orientation of conjugated AMPs could be investigated in future studies.[26,66]

### Effect of the Cross-Linker Concentration on Function.

The effect of the cross-linker concentration was investigated to test antimicrobial activity of AMPM3-polymer conjugates. Both peptide control-5 and polymer-only-5 to polymer-only-20 (polymer conjugates with 20% cross-linker) controls did not inhibit the growth of *S. mutans.* The cross-linker concentration of polymer-only controls did not affect the lack of antimicrobial activity. MA-AMPM3–5, MA-AMPM3–10, and MA-AMPM3–15 inhibited the growth of *S. mutans* in Figure 4 by nearly 80%, 70%, and 50%, respectively. MA-AMPM3–20 discs did not show significant inhibition against *S. mutans* (Figure 4). The inhibitory effect was reduced as the cross-linker concentration increased; it may be plausible that increased network composition may have restricted the conjugated AMP's access to the bacteria.

Previous studies have found that the bond durability may be affected by the differing mechanical properties of specific adhesive formulations.[80–84] We investigated critical mechanical properties for our engineered AMP-polymer conjugates. Compression, tensile, and rheological studies have been widely used to determine the mechanical properties.[46,85–89] For this study, compression tests were performed to analyze the viscoelastic behaviors of the control specimens and obtain the stress–strain curves (Figure 5). Although the compressive modulus alone does not directly inform about tensile performance, it is still consistent with the claim that AMP conjugation does not compromise the mechanical strength of the adhesive polymer. With the increase in the cross-linker, TEGDMA, concentration from 5, 10, 15, to 20 wt %, the Young's moduli of the control samples were found to be 1.8 ± 0.1, 5.2 ± 0.4, 9.4 ± 0.2, and 16.2 ± 0.4 MPa, respectively. The corresponding AMP-polymer conjugates showed Young's moduli from 2.4 ± 0.3, 5.1 ± 0.2, 9.1 ± 0.5, and 16.6 ± 0.5 MPa, respectively, across the same cross-linker concentration range. The Young's modulus was either higher for AMP-polymer conjugates or within the observed error of control polymers. The addition of conjugated AMP by itself does not directly lead to a loss of stiffness of the tested adhesive materials. Compared to the modulus of the polyHEMA-only hydrogel (0.2 MPa, see Figure S3), our AMP-polymer conjugate specimens achieved a strength 10–100 times greater.

## CONCLUSION

Compared to existing approaches in the dental adhesive field, AMPs offer a promising solution for the dental composite restoration failure. To address the vulnerable adhesive–dentin interface, we designed a tunable AMP-based adhesive system with inherent antimicrobial activity against a key pathogen for dental caries. The spacer-integrated antimicrobial peptides were conjugated to methacrylate (MA), and the resulting MA-AMP monomers were next copolymerized into dental adhesives. We investigated two different

spacer sequences to provide conformational flexibility during conjugation to the adhesive polymer. AMP-adhesive polymer with a GGG spacer had significantly more activity than the AMP-adhesive polymer with a SSSGGG spacer. We use computationally generated secondary-structure ensembles to estimate the changes in secondary structure of the active antimicrobial peptide domain based on the selected spacer sequences. The GGG spacer produced less secondary structural feature shifts than the SSSGGG spacer. The conformational shift effect may result in improved functionality of the active domain if the secondary structures related to activity become more frequent following combining the spacer domain. Our results show that spacer engineering provides an opportunity to tune the activity of the peptide in the system. We next studied the cross-linker concentration effect on the mechanical property in engineered AMP-integrated dental adhesives. The Young's modulus was found to be either higher for AMP-polymer conjugates such as polyHEMA or within the observed error of control polymers. Our peptide structure–function analyses indicated engineered spacer peptide sequences may also be incorporated via additional or alternative functional groups to integrate active peptides into any variety of monomer/polymer combinations. Incorporating antibacterial activity within a dental adhesive as part of the polymerization step provides a path for integrating various biological functions at the interface of hybrid soft materials. The proposed adhesive integrating biofunctionalities into a dental adhesive material design opens up opportunities for multitude of applications ranging from tissue engineering to drug delivery to food technologies and beyond. Conjugating the peptide by using an engineered spacer sequences opens a new path to integrate multiple, distinct peptide sequences with conformational stability and control their spatial distribution in the composite material. The approach could be expanded toward integrating multi-biomolecular activity into polymeric materials beyond the single phase. In the recent years, nanoscaled fibers have been increasingly shown as effective drug delivery vehicles.[90] Applying our technology to biphasic systems such as core–sheath fibers would offer to control biphasic drug release, providing antimicrobial with antiinflammatory and/or antihistaminic properties.[91] Various innovative functional materials may be designed and exploited in a wide variety of applications including, but not limited to, the treatment of secondary caries, enhanced durability of dental composite restorations, antimicrobial gels, and tissue engineering approaches.

## Supplementary Material

Refer to Web version on PubMed Central for supplementary material.

## ACKNOWLEDGMENTS

This work was supported by research grant R01DE025476 (P.S., C.T.) from the National Institute of Dental and Craniofacial Research, National Institutes of Health, Bethesda, MD.

## REFERENCES

(1). Delaviz Y; Finer Y; Santerre JP Biodegradation of Resin Composites and Adhesives by Oral Bacteria and Saliva: A Rationale for New Material Designs that Consider the Clinical Environment and Treatment Challenges. Dent. Mater 2014, 30 (1), 16–32. [PubMed: 24113132]

(2). Moszner N; Hirt T New Polymer-Chemical Developments in Clinical Dental Polymer Materials: Enamel—Dentin Adhesives and Restorative Composites. J. Polym. Sci., Part A: Polym. Chem 2012, 50 (21), 4369–4402.

(3). Santerre J; Shajii L; Leung B Relation of Dental Composite Formulations to Their Degradation and the Release of Hydrolyzed Polymeric-Resin-Derived Products. Crit. Rev. Oral Biol. Med 2001, 12 (2), 136–151. [PubMed: 11345524]

(4). Rho YJ; Namgung C; Jin BH; Lim BS; Cho BH Longevity of Direct Restorations in Stress-Bearing Posterior Cavities: A Retrospective Study. Oper. Dent 2013, 38 (6), 572–82. [PubMed: 23550914]

(5). Bernardo M; Luis H; Martin MD; Leroux BG; Rue T; Leitao J; DeRouen TA Survival and Reasons for Failure of Amalgam versus Composite Posterior Restorations Placed in a Randomized Clinical Trial. J. Am. Dent. Assoc., JADA 2007, 138 (6), 775–783. [PubMed: 17545266]

(6). Spencer P; Ye Q; Misra A; Goncalves S. d. P.; Laurence J Proteins, Pathogens, and Failure at the Composite-Tooth Interface. J. Dent. Res 2014, 93 (12), 1243–1249. [PubMed: 25190266]

(7). Van de Sande F; Collares K; Correa M; Cenci M; Demarco F; Opdam N Restoration Survival: Revisiting Patients' Risk Factors through a Systematic Literature Review. Oper. Dent 2016, 41 (S7), S7–S26. [PubMed: 27689931]

(8). Astvaldsdottir A; Dagerhamn J; van Dijken JW; Naimi-Akbar A; Sandborgh-Englund G; Tranaeus S; Nilsson M Longevity of Posterior Resin Composite Restorations in Adults - A Systematic Review. J. Dent 2015, 43 (8), 934–54. [PubMed: 26003655]

(9). Zhou Y; Shimada Y; Matin K; Sadr A; Sumi Y; Tagami J Assessment of Bacterial Demineralization around Composite Restorations using Swept-Source Optical Coherence Tomography (SS-OCT). Dent. Mater 2016, 32 (9), 1177–1188. [PubMed: 27435052]

(10). Gregory RL; El-Rahman A; Avery D Effect of Restorative Treatment on Mutans Streptococci and IgA antibodies. Pediatr. Dent 1998, 20, 273–277. [PubMed: 9783299]

(11). Takahashi N; Nyvad B The Role of Bacteria in the Caries Process: Ecological Perspectives. J. Dent. Res 2011, 90 (3), 294–303. [PubMed: 20924061]

(12). Horie K; Shimada Y; Matin K; Ikeda M; Sadr A; Sumi Y; Tagami J Monitoring of Cariogenic Demineralization at the Enamel-Composite Interface using Swept-Source Optical Coherence Tomography. Dent. Mater 2016, 32 (9), 1103–1112. [PubMed: 27427292]

(13). Bertassoni LE; Orgel JP; Antipova O; Swain MV The Dentin Organic Matrix-Limitations of Restorative Dentistry Hidden on the Nanometer Scale. Acta Biomater. 2012, 8 (7), 2419–2433. [PubMed: 22414619]

(14). Pandit S; Kim J-E; Jung K-H; Chang K-W; Jeon J-G Effect of Sodium Fluoride on the Virulence Factors and Composition of Streptococcus mutans Biofilms. Arch. Oral Biol 2011, 56 (7), 643–649. [PubMed: 21241981]

(15). Zhang K; Cheng L; Imazato S; Antonucci JM; Lin NJ; Lin-Gibson S; Bai Y; Xu HH Effects of Dual Antibacterial Agents MDPB and Nano-Silver in Primer on Microcosm Biofilm, Cytotoxicity and Dentine Bond Properties. J. Dent 2013, 41 (5), 464–474. [PubMed: 23402889]

(16). Liu C; Faria AF; Ma J; Elimelech M Mitigation of Biofilm Development on Thin-Film Composite Membranes Functionalized with Zwitterionic Polymers and Silver Nanoparticles. Environ. Sci. Technol 2017, 51 (1), 182–191. [PubMed: 27976869]

(17). Zhang N; Ma J; Melo MA; Weir MD; Bai Y; Xu HH Protein-Repellent and Antibacterial Dental Composite to Inhibit Biofilms and Caries. J. Dent 2015, 43 (2), 225–234. [PubMed: 25478889]

(18). Brambilla E; Ionescu A; Fadini L; Mazzoni A; Imazato S; Pashley D; Breschi L; Gagliani M Influence of MDPB-containing primer on Streptococcus mutans biofilm formation in simulated Class I restorations. J. Adhes. Dent 2013, 15 (5), 431–438. [PubMed: 23534020]

(19). Schwaiger K; Harms KS; Bischoff M; Preikschat P; Mölle G; Bauer-Unkauf I; Thalhammer S; Bauer J; Holzel CS Insusceptibility to Disinfectants in Bacteria from Animals, Food and Humans —Is There a Link to Antimicrobial Resistance? Front. Microbiol 2014, 5, 88. [PubMed: 24672513]

(20). Bragg R; Jansen A; Coetzee M; van der Westhuizen W; Boucher C Bacterial Resistance to Quaternary Ammonium Compounds (QAC) Disinfectants. In Infectious Diseases and Nanomedicine II; Springer: 2014; pp 1–13.

(21). Dobson A; O'connor P; Cotter P; Ross R; Hill C Impact of the Broad-Spectrum Antimicrobial Peptide, Lacticin 3147, on Streptococcus mutans Growing in a Biofilm and in Human Saliva. J. Appl Microbiol 2011, 111 (6), 1515–1523. [PubMed: 21923747]

(22). Wang W; Tao R; Tong Z; Ding Y; Kuang R; Zhai S; Liu J; Ni L Effect of a Novel Antimicrobial Peptide Chrysophsin-1 on Oral Pathogens and Streptococcus mutans Biofilms. Peptides 2012, 33 (2) , 212–219. [PubMed: 22281025]

(23). Li H; Cheng JW; Yu HY; Xin Y; Tang L; Ma Y Effect of the Antimicrobial Peptide D-Nal-Pac-525 on the Growth of Streptococcus mutans and Its Biofilm Formation. J. Microbiol. Biotechnol 2013, 23 (8), 1070–1075. [PubMed: 23711527]

(24). Shang D; Liang H; Wei S; Yan X; Yang Q; Sun Y Effects of Antimicrobial Peptide L-K6, A Temporin-1ceb Analog on Oral Pathogen Growth, Streptococcus mutans Biofilm Formation, and Anti-Inflammatory Activity. Appl. Microbiol. Biotechnol 2014, 98 (20), 8685–8695. [PubMed: 25056289]

(25). Sanchez-Gomez S; Martinez-de-Tejada G Antimicrobial Peptides as Anti-Biofilm Agents in Medical Implants. Curr. Top. Med. Chem 2016, 17 (5), 590–603.

(26). Yazici H; O'Neill MB; Kacar T; Wilson BR; Oren EE; Sarikaya M; Tamerler C. Engineered Chimeric Peptides as Antimicrobial Surface Coating Agents Toward Infection-Free Implants. ACS Appl. Mater. Interfaces 2016, 8 (8), 5070–5081. [PubMed: 26795060]

(27). Holmberg KV; Abdolhosseini M; Li Y; Chen X; Gorr SU; Aparicio C Bio-inspired Stable Antimicrobial Peptide Coatings for Dental Applications. Acta Biomater. 2013, 9 (9), 8224–31. [PubMed: 23791670]

(28). Aida K; Kreling P; Caiaffa K; Calixto G; Chorilli M; Spolidorio D; Santos-Filho N; Cilli EM; Duque C Antimicrobial Peptide-Loaded Liquid Crystalline Precursor Bioadhesive System for the Prevention of Dental Caries. Int. J. Nanomed 2018, 13, 3081–3091.

(29). Xie S-X; Boone K; VanOosten SK; Yuca E; Song L; Ge X; Ye Q; Spencer P; Tamerler C Peptide Mediated Antimicrobial Dental Adhesive System. Appl. Sci 2019, 9 (3), 557. [PubMed: 33542835]

(30). Mai S; Mauger MT; Niu LN; Barnes JB; Kao S; Bergeron BE; Ling JQ; Tay FR Potential Applications of Antimicrobial Peptides and Their Mimics in Combating Caries and Pulpal Infections. Acta Biomater. 2017, 49, 16–35. [PubMed: 27845274]

(31). González-Henríquez C; Sarabia-Vallejos M; Rodriguez-Hernandez J Advances in the Fabrication of Antimicrobial Hydrogels for Biomedical Applications. Materials 2017, 10 (3), 232.

(32). Malmsten M Antimicrobial and Antiviral Hydrogels. Soft Matter 2011, 7 (19), 8725–8736.

(33). Babavalian H; Latifi AM; Shokrgozar MA; Bonakdar S; Mohammadi S; Moghaddam MM Analysis of Healing Effect of Alginate Sulfate Hydrogel Dressing Containing Antimicrobial Peptide on Wound Infection Caused By Methicillin-Resistant Staphylococcus aureus. Jundishapur J. Microbiol 2015, 8 (9), No. e28320. [PubMed: 26487923]

(34). Silva J; Dhall S; Chan A; Gama M; Mgreen M Improved Burn Wound Healing By An Antimicrobial Peptide Released From Conjugates With Dextrin Embedded In A Carbopol Hydrogel. Wound Repair Regen. 2015, 23 (2), A40.

(35). Xie Z; Aphale NV; Kadapure TD; Wadajkar AS; Orr S; Gyawali D; Qian G; Nguyen KT; Yang J Design of Antimicrobial Peptides Conjugated Biodegradable Citric Acid Derived Hydrogels for Wound Healing. J. Biomed. Mater. Res., Part A 2015, 103 (12), 3907–3918.

(36). Wang R; Xu D.-l.; Liang L; Xu T.-t; Liu W; Ouyang P.-k.; Chi B; Xu H. Enzymatically Crosslinked Epsilon-Poly-L-Lysine Hydrogels with Inherent Antibacterial Properties for Wound Infection Prevention. RSC Adv. 2016, 6 (11), 8620–8627.

(37). Buffet-Bataillon S; Tattevin P; Bonnaure-Mallet M; Jolivet-Gougeon A Emergence of Resistance to Antibacterial Agents: The Role of Quaternary Ammonium Compounds—A Critical Review. Int. J. Antimicrob. Agents 2012, 39 (5), 381–389. [PubMed: 22421329]

(38). Kumar P; Takayesu A; Abbasi U; Kalathottukaren MT; Abbina S; Kizhakkedathu JN; Straus SK Antimicrobial Peptide–Polymer Conjugates with High Activity: Influence of Polymer Molecular Weight and Peptide Sequence on Antimicrobial Activity, Proteolysis, and Biocompatibility. ACS Appl. Mater. Interfaces 2017, 9 (43), 37575–37586. [PubMed: 29019386]

(39). Cheng JTJ; Hale JD; Kindrachuk J; Jessen H; Elliott M; Hancock REW; Straus SK. Importance of Residue 13 and the C-Terminus for the Structure and Activity of the Antimicrobial Peptide Aurein 2.2. Biophys. J 2010, 99 (9), 2926–2935. [PubMed: 21044590]

(40). Cheng JT; Hale JD; Elliot M; Hancock RE; Straus SK Effect of Membrane Composition on Antimicrobial Peptides Aurein 2.2 and 2.3 from Australian Southern Bell Frogs. Biophys. J 2009, 96 (2), 552–65. [PubMed: 19167304]

(41). Wilson P Synthesis and Applications of Protein/Peptide-Polymer Conjugates. Macromol. Chem. Phys 2017, 218 (9), 1600595.

(42). Heredia KL; Maynard HD Synthesis of Protein-Polymer Conjugates. Org. Biomol. Chem 2007, 5 (1), 45–53. [PubMed: 17164904]

(43). Sun H; Hong Y; Xi Y; Zou Y; Gao J; Du J Synthesis, Self-Assembly, and Biomedical Applications of Antimicrobial Peptide–Polymer Conjugates. Biomacromolecules 2018, 19 (6), 1701–1720. [PubMed: 29539262]

(44). Nichol JW; Koshy ST; Bae H; Hwang CM; Yamanlar S; Khademhosseini A Cell-Laden Microengineered Gelatin Methacrylate Hydrogels. Biomaterials 2010, 31 (21), 5536–5544. [PubMed: 20417964]

(45). Annabi N; Rana D; Sani ES; Portillo-Lara R; Gifford JL; Fares MM; Mithieux SM; Weiss AS Engineering a Sprayable and Elastic Hydrogel Adhesive with Antimicrobial Properties for Wound Healing. Biomaterials 2017, 139, 229–243. [PubMed: 28579065]

(46). Yi X; He J; Wang X; Zhang Y; Tan G; Zhou Z; Chen J; Chen D; Wang R; Tian W; Yu P; Zhou L; Ning C Tunable Mechanical, Antibacterial, and Cytocompatible Hydrogels Based on a Functionalized Dual Network of Metal Coordination Bonds and Covalent Crosslinking. ACS Appl. Mater. Interfaces 2018, 10 (7), 6190–6198. [PubMed: 29381319]

(47). Song A; Rane AA; Christman KL Antibacterial and Cell-Adhesive Polypeptide and Poly (Ethylene Glycol) Hydrogel as a Potential Scaffold for Wound Healing. Acta Biomater. 2012, 8 (1), 41–50. [PubMed: 22023748]

(48). Gavel PK; Dev D; Parmar HS; Bhasin S; Das AK Investigations of Peptide-Based Biocompatible Injectable Shape-Memory Hydrogels: Differential Biological Effects on Bacterial and Human Blood Cells. ACS Appl. Mater. Interfaces 2018, 10 (13), 10729–10740. [PubMed: 29537812]

(49). Shams Es-haghi S; Mayfield MB; Weiss R Effect of Freeze/Thaw Process on Mechanical Behavior of Double-Network Hydrogels in Finite Tensile Deformation. Macromolecules 2018, 51 (3), 1052–1057.

(50). Papadogiannis D; Lakes RS; Papadogiannis Y; Tolidis K Mechanical Viscoelastic Behavior of Dental Adhesives. Dent. Mater 2013, 29 (6), 693–701. [PubMed: 23601583]

(51). Hosaka K; Nakajima M; Takahashi M; Itoh S; Ikeda M; Tagami J; Pashley DH Relationship Between Mechanical Properties of One-Step Self-Etch Adhesives and Water Sorption. Dent. Mater 2010, 26 (4), 360–7. [PubMed: 20053432]

(52). Imazato S; Kinomoto Y; Tarumi H; Torii M; Russell R; McCabe J Incorporation of Antibacterial Monomer MDPB into Dentin Primer. J. Dent. Res 1997, 76 (3), 768–772. [PubMed: 9109826]

(53). Cocco AR; de Oliveira da Rosa WL; da Silva AF; Lund RG; Piva E. A Systematic Review about Antibacterial Monomers used in Dental Adhesive Systems: Current Status and Further Prospects. Dent. Mater 2015, 31 (11), 1345–1362. [PubMed: 26345999]

(54). Jennings MC; Minbiole KP; Wuest WM Quaternary Ammonium Compounds: An Antimicrobial Mainstay and Platform for Innovation to Address Bacterial Resistance. ACS Infect. Dis 2015, 1 (7), 288–303. [PubMed: 27622819]

(55). Team EE CDC Publishes Report On Antibiotic Resistance Threats In The United States For The First Time. Euro Surveillance: European Communicable Disease Bulletin, 2013; 18 (38).

(56). Koczulla AR; Bals R Antimicrobial Peptides. Drugs 2003, 63 (4), 389–406. [PubMed: 12558461]

(57). Su M; Yao S; Gu L; Huang Z; Mai S Antibacterial Effect and Bond Strength of a Modified Dental Adhesive Containing the Peptide Nisin. Peptides 2018, 99, 189–194. [PubMed: 29024714]

(58). de Arauz LJ; Jozala AF; Mazzola PG; Penna TCV Nisin Biotechnological Production And Application: A Review. Trends Food Sci. Technol 2009, 20 (3–4), 146–154.

(59). Tu H; Fan Y; Lv X; Han S; Zhou X; Zhang L Activity of Synthetic Antimicrobial Peptide GH12 Against Oral Streptococci. Caries Res. 2016, 50 (1), 48–61. [PubMed: 26859135]

(60). Wang Y; Wang X; Jiang W; Wang K; Luo J; Li W; Zhou X; Zhang L Antimicrobial Peptide GH12 Suppresses Cariogenic Virulence Factors of Streptococcus mutans. J. Oral Microbiol 2018, 10 (1), 1442089. [PubMed: 29503706]

(61). Wang Y; Zeng Y; Wang Y; Li H; Yu S; Jiang W; Li Y; Zhang L Antimicrobial Peptide GH12 Targets Streptococcus mutans to Arrest Caries Development in Rats. J. Oral Microbiol 2019, 11 (1), 1549921.

(62). Moussa DG; Kirihara JA; Ye Z; Fischer NG; Khot J; Witthuhn BA; Aparicio C Dentin Priming with Amphipathic Antimicrobial Peptides. J. Dent. Res 2019, 98 (10), 1112–1121. [PubMed: 31313946]

(63). Moussa DG; Fok A; Aparicio C Hydrophobic and Antimicrobial Dentin: A Peptide-Based 2-Tier Protective System for Dental Resin Composite Restorations. Acta Biomater. 2019, 88, 251–265. [PubMed: 30753942]

(64). Fjell CD; Hiss JA; Hancock REW; Schneider G Designing Antimicrobial Peptides: Form Follows Function. Nat. Rev. Drug Discovery 2012, 11 (1), 37–51.

(65). Yucesoy DT; Hnilova M; Boone K; Arnold PM; Snead ML; Tamerler C Chimeric Peptides as Implant Functionalization Agents for Titanium Alloy Implants with Antimicrobial Properties. JOM 2015, 67 (4), 754–766. [PubMed: 26041967]

(66). Wisdom C; VanOosten SK; Boone KW; Khvostenko D; Arnold PM; Snead ML; Tamerler C Controlling the Biomimetic Implant Interface: Modulating Antimicrobial Activity by Spacer Design. J. Mol. Eng. Mater 2016, 4 (01), 1640005. [PubMed: 28936427]

(67). Sarma D; Hajovsky H; Koen YM; Galeva NA; Williams TD; Staudinger JL; Hanzlik RP Covalent Modification of Lipids and Proteins in Rat Hepatocytes and In Vitro by Thioacetamide Metabolites. Chem. Res. Toxicol 2012, 25 (9), 1868–1877. [PubMed: 22667464]

(68). Ge X; Ye Q; Song L; Misra A; Spencer P The Influence of Water on Visible-Light Initiated Free-Radical/Cationic Ring-Opening Hybrid Polymerization of Methacrylate/Epoxy: Polymerization Kinetics, Crosslinking Structure and Dynamic Mechanical Properties. RSC Adv. 2015, 5 (95), 77791–77802. [PubMed: 26613015]

(69). VanOosten SK; Yuca E; Karaca BT; Boone K; Snead ML; Spencer P; Tamerler C Biosilver Nanoparticle Interface Offers Improved Cell Viability. Surf. Innovations 2016, 4 (3), 121.

(70). Ferraro MJ Methods for Dilution Antimicrobial Susceptibility Tests for Bacteria That Grow Aerobically; NCCLS: 2000.

(71). Min KR; Galvis A; Williams B; Rayala R; Cudic P; Ajdic D Antibacterial and Antibiofilm Activities of a Novel Synthetic Cyclic Lipopeptide Against Cariogenic Streptococcus mutans UA159. Antimicrob. Agents Chemother 2017, 61 (8), e00776–17. [PubMed: 28533236]

(72). Nociari MM; Shalev A; Benias P; Russo C A Novel One-Step, Highly Sensitive Fluorometric Assay to Evaluate Cell-Mediated Cytotoxicity. J. Immunol. Methods 1998, 213 (2), 157–167. [PubMed: 9692848]

(73). Page B; Page M; Noel C A New Fluorometric Assay for Cytotoxicity Measurements In-Vitro. Int. J. Oncol 1993, 3 (3), 473–476. [PubMed: 21573387]

(74). Song L; Ye Q; Ge X; Misra A; Laurence JS; Berrie CL; Spencer P Synthesis and Evaluation of Novel Dental Monomer with Branched Carboxyl Acid Group. J. Biomed. Mater. Res. Part B 2014, 102 (7), 1473–1484.

(75). Kim DE; Chivian D; Baker D Protein Structure Prediction And Analysis Using The Robetta Server. Nucleic Acids Res. 2004, 32, 526–531.

(76). Kabsch W; Sander C DSSP: Definition of Secondary Structure of Proteins Given a Set of 3D Coordinates. Biopolymers 1983, 22, 2577–2637. [PubMed: 6667333]

(77). Sedlak RH; Hnilova M; Grosh C; Fong H; Baneyx F; Schwartz D; Sarikaya M; Tamerler C; Traxler B Engineered Escherichia coli Silver-Binding Periplasmic Protein That Promotes Silver Tolerance. Appl. Environ. Microbiol 2012, 78 (7), 2289–2296. [PubMed: 22286990]

(78). Miles AJ; Wallace BA Circular Dichroism Spectroscopy of Membrane Proteins. Chem. Soc. Rev 2016, 45 (18), 4859–4872. [PubMed: 27347568]

(79). Liu Z; Ma S; Duan S; Xuliang D; Sun Y; Zhang X; Xu X; Guan B; Wang C; Hu M; Qi X; Zhang X; Gao P Modification of Titanium Substrates with Chimeric Peptides Comprising Antimicrobial and Titanium-Binding Motifs Connected by Linkers To Inhibit Biofilm Formation. ACS Appl. Mater. Interfaces 2016, 8 (8), 5124–36. [PubMed: 26863404]

(80). De Munck J. d.; Van Landuyt K; Peumans M; Poitevin A; Lambrechts P; Braem M; Van Meerbeek B A Critical Review of the Durability of Adhesion to Tooth Tissue: Methods and Results. J. Dent. Res 2005, 84 (2), 118–132. [PubMed: 15668328]

(81). Tsujimoto A; Barkmeier WW; Takamizawa T; Watanabe H; Johnson WW; Latta MA; Miyazaki M Relationship Between Mechanical Properties and Bond Durability of Short Fiber-Reinforced Resin Composite with Universal Adhesive. Eur. J. Oral Sci 2016, 124 (5), 480–489. [PubMed: 27696555]

(82). Yahyazadehfar M; Mutluay MM; Majd H; Ryou H; Arola D Fatigue of the Resin-Enamel Bonded Interface and the Mechanisms of Failure. J. Mech. Behav. Biomed. Mater 2013, 21, 121–132. [PubMed: 23571321]

(83). Mutluay MM; Yahyazadehfar M; Ryou H; Majd H; Do D; Arola D Fatigue of the Resin-Dentin Interface: A New Approach for Evaluating the Durability of Dentin Bonds. Dent. Mater 2013, 29 (4), 437–449. [PubMed: 23434232]

(84). Carvalho RM; Manso AP; Geraldeli S; Tay FR; Pashley DH Durability of Bonds and Clinical Success of Adhesive Restorations. Dent. Mater 2012, 28 (1), 72–86. [PubMed: 22192252]

(85). Guven MN; Altuncu MS; Bal T; Oran DC; Gulyuz U; Kizilel S; Okay O; Avci D Bisphosphonic Acid-Functionalized Cross-Linkers to Tailor Hydrogel Properties for Biomedical Applications. ACS Omega 2018, 3 (8), 8638–8647. [PubMed: 31458994]

(86). Singh B; Sharma S; Dhiman A Design of Antibiotic Containing Hydrogel Wound Dressings: Biomedical Properties and Histological Study of Wound Healing. Int. J. Pharm 2013, 457 (1), 82–91. [PubMed: 24075861]

(87). Hobzova R; Hrib J; Sirc J; Karpushkin E; Michalek J; Janouskova O; Gatenholm P Embedding of Bacterial Cellulose Nanofibers within PHEMA Hydrogel Matrices: Tunable Stiffness Composites with Potential for Biomedical Applications. J. Nanomater 2018, 2018, 1–12.

(88). Baral A; Roy S; Ghosh S; Hermida-Merino D; Hamley IW; Banerjee A A Peptide-Based Mechano-Sensitive, Proteolytically Stable Hydrogel with Remarkable Antibacterial Properties. Langmuir 2016, 32 (7), 1836–1845. [PubMed: 26818698]

(89). Veiga AS; Sinthuvanich C; Gaspar D; Franquelim HG; Castanho MA; Schneider JP Arginine-Rich Self-Assembling Peptides as Potent Antibacterial Gels. Biomaterials 2012, 33 (35), 8907–8916. [PubMed: 22995710]

(90). Heseltine PL; Ahmed J; Edirisinghe M Developments in Pressurized Gyration for the Mass Production of Polymeric Fibers. Macromol Mater. Eng 2018, 303 (9), 1800218.

(91). Mahalingam S; Homer-Vanniasinkam S; Edirisinghe M Novel Pressurised Gyration Device for Making Core-Sheath Polymer Fibres. Mater. Des 2019, 178, 107846.

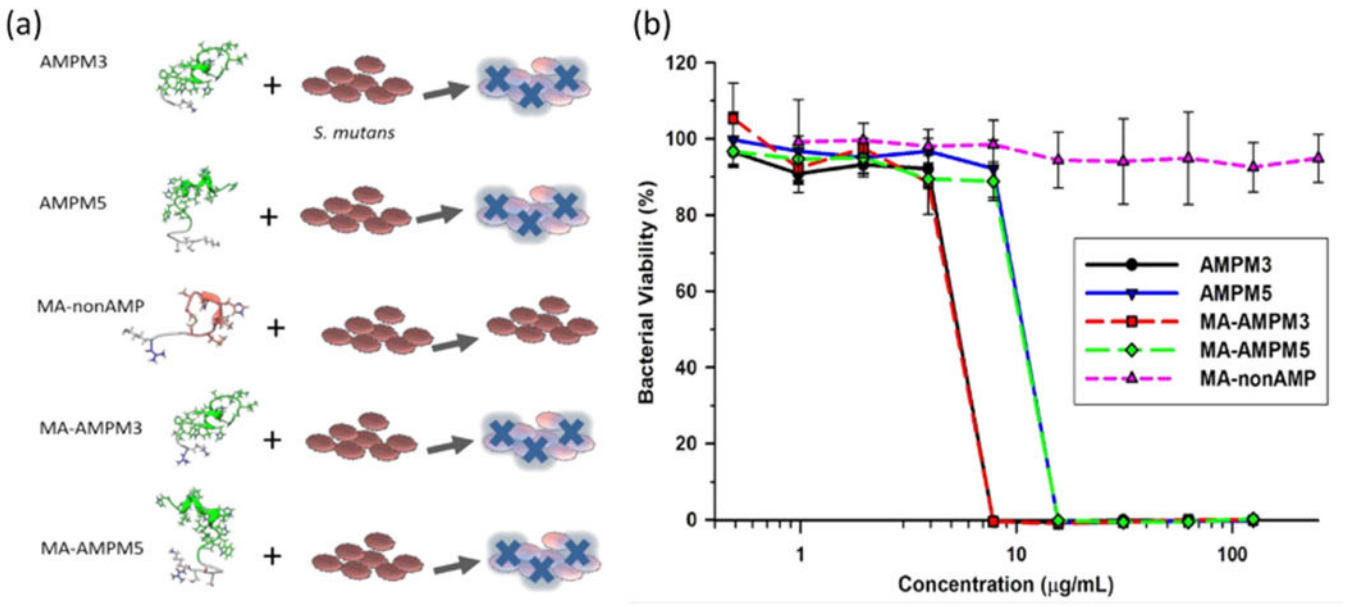


**Figure 1.**

Schematic illustration (a) and graphical representation (b) of antibacterial activity of AMPs, AMP-monomers, and non-AMP-monomer (MA-non-AMP).

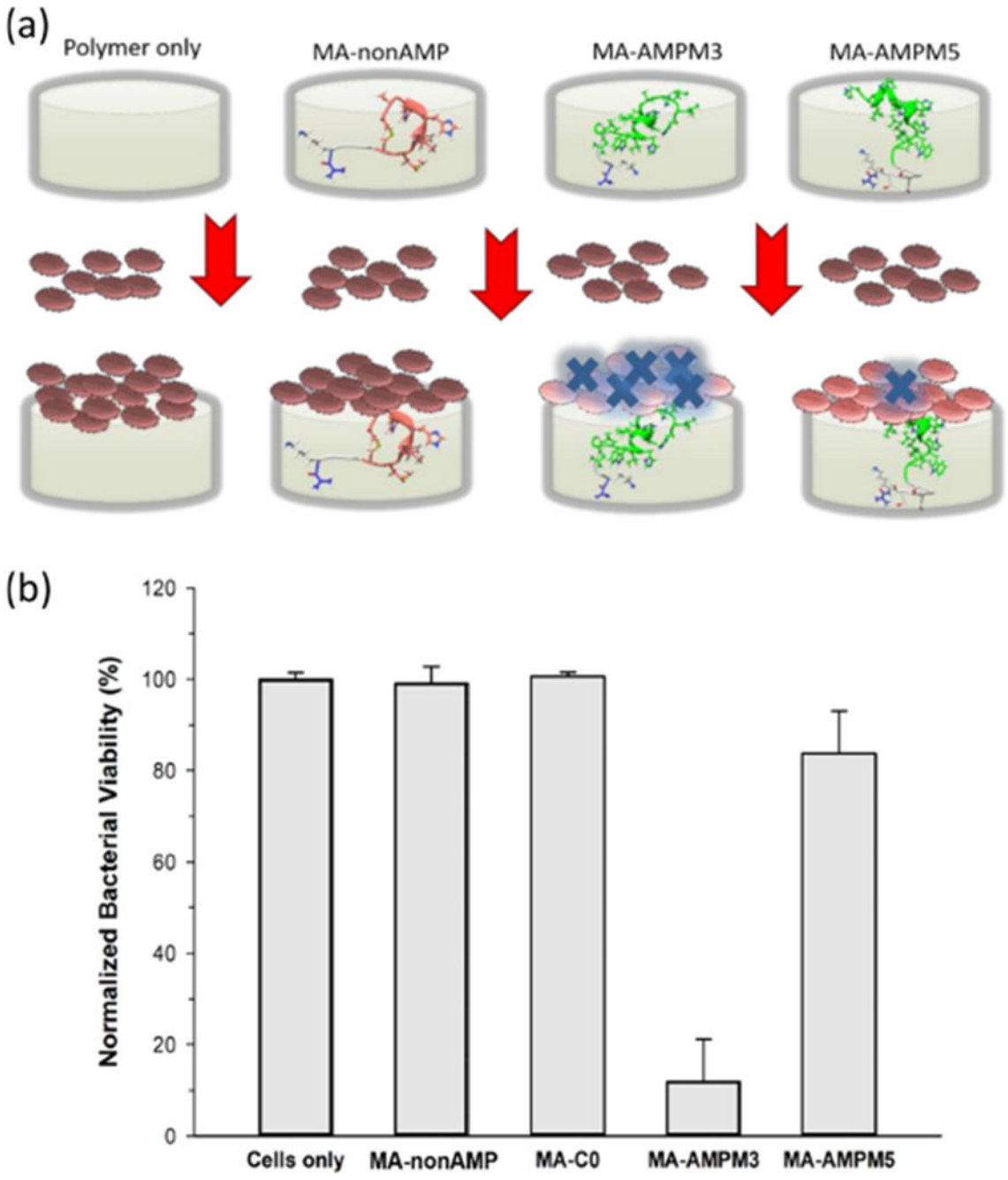


**Figure 2.**

Schematic illustration (a) and graphical representation (b) of the viability of *S. mutans* cultures after overnight incubation with polymerized discs containing non-AMP-monomer and AMP-monomers. *S. mutans*: a positive control without a disc. Peptide control: MA-non-AMP with GGG as a spacer. MA-C0 is the methacrylate control polymer replacing methacrylate peptide conjugates with methacrylate monomer.

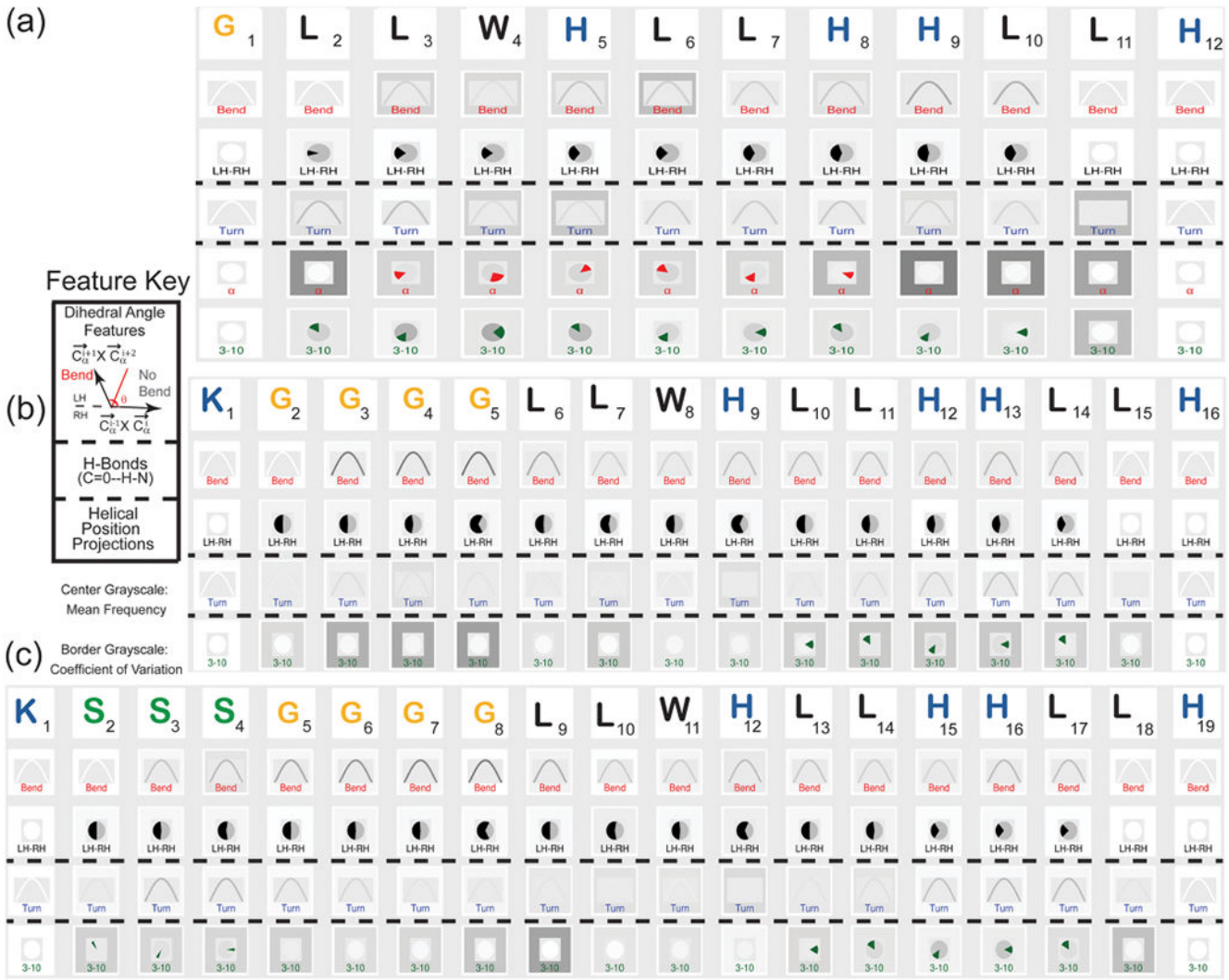


**Figure 3.**

Residue-based flexibility and structural features for AMPs modeled by the PyRosetta peptide-folding script and labeled with DSSP. The top panel shows GH12, the antimicrobial peptide domain by itself. The middle panel shows AMPM3, the GH12 variant with a KGGG spacer. The bottom panel shows AMPM5, the GH12 variant with KSSSGGG spacer. The first row of the grid in each panel is the residue letter and residue number as the bend row. The color coding for the residue letter is by amino acid type: glycine = yellow, polar = green, charged residue = blue, and nonpolar = black. The row key starts with the first row below the residue letters, which is the bend row. The bend row is defined by the dihedral angle of the planes formed by $\alpha$ carbons of neighboring residues. The row key arrow pointing to the right-hand side of the page is in the direction of the cross-product of the position vectors for these two $\alpha$ carbons. The second arrow is the direction of the cross product of the $\alpha$ carbon position vectors for residues ($i + 1$) and ($i + 2$). A bend exists at a residue if this angle is greater than 70°. Across the panels, the grayscale of the center portion refers to the mean frequency of the feature, and the grayscale of the border refers to the coefficient of variation of across the ensembles, with black corresponding to 100%. The LH-

RH panel describes the sign of the dihedral angle (left-hand indicates an angle less than 180°, while the RH indicates one greater.) The grayscale portion of the pie indicates the proportion of right-hand dihedral angles. A turn, in the row below, exists at a residue if backbone carbonyl hydrogen bonds to an adjacent backbone amide. Helices are one type of hydrogen bond pattern. Helical projections are provided by residue position to determine which residue share the same helical face. The colored portion describes the projection, while the grayscale portion shows the mean frequency.

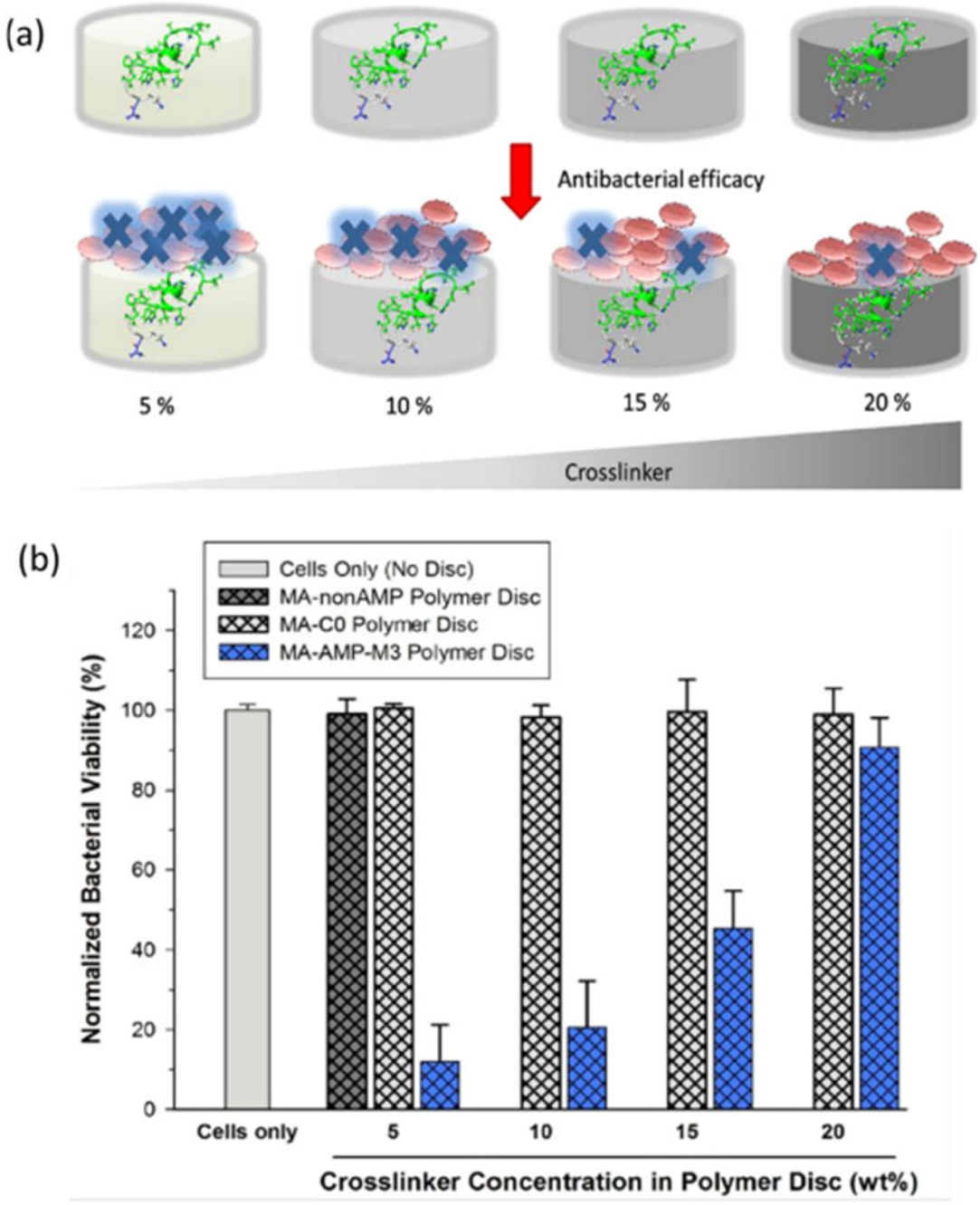


**Figure 4.**

Schematic illustration (a) and the graphical presentation (b) of the viability of *S. mutans* cultures after overnight incubation with polymerized discs containing different cross-linker concentration. *S. mutans*: a positive control without a disc. Peptide control: MA-non-AMP with GGG as a spacer.

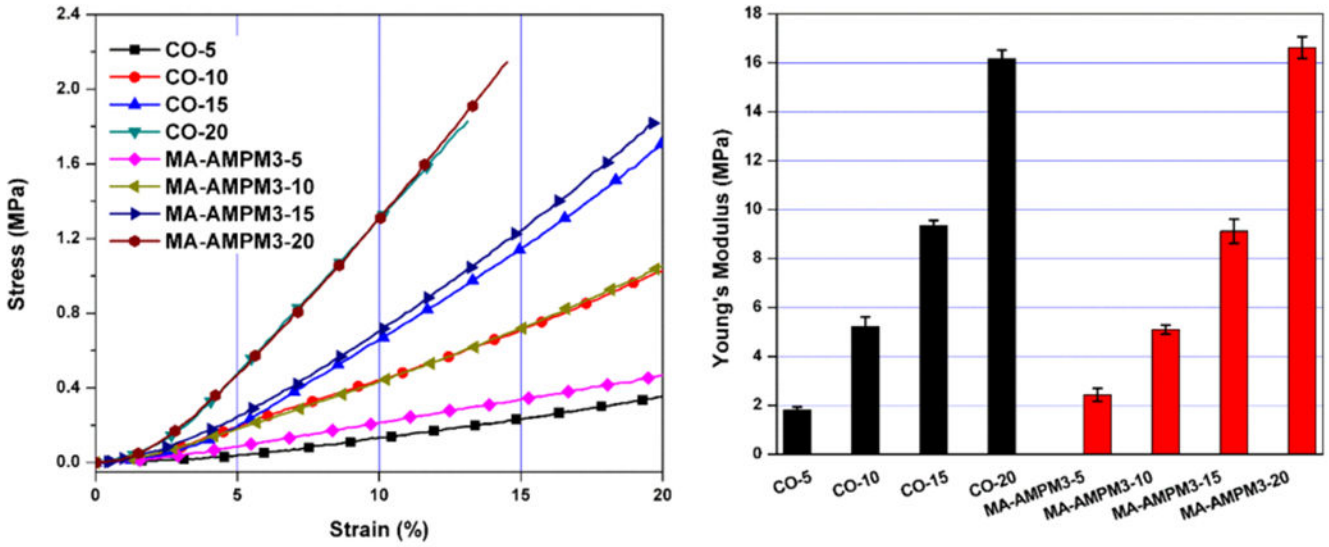


**Figure 5.**

Representative stress–strain curves from compression test and bar figure of the Young's moduli of the controls and AMP-polymer conjugates cylindrical samples.

**Table 1.**

Properties of Synthesized Peptide Materials: Antimicrobial Peptides (AMPs), AMP-Monomers, and Non-AMP-Monomer[a]

| denotation | sequence | $IC_{50}$ ($\mu$g/mL) | MIC ($\mu$g/mL) | calculated MW (Da) | observed MW (Da) |
|---|---|---|---|---|---|
| AMPM3 | K_GGG_GLLWHLLHHLLH-$CONH_2$ | 5.0 | 7.8 | 1787.1 | 1787.0 |
| AMPM5 | K_SSSGGG_GLLWHLLHHLLH-$CONH_2$ | 8.8 | 15.6 | 2048.4 | 2048.1 |
| MA-AMPM3 | MA-K_GGG_GLLWHLLHHLLH-$CONH_2$ | 4.8 | 7.8 | 1855.2 | 1855.1 |
| MA-AMPM5 | MA-K_SSSGGG_GLLWHLLHHLLH-$CONH_2$ | 10.0 | 15.6 | 2115.4 | 2115.1 |
| MA-non-AMP | MA-K_GGG_CMLPHHGAC | >250[b] | >250[b] | 1334.6 | 1335.4 |

[a]The observed molecular weight was experimentally derived by mass spectrometry.

[b]250 $\mu$g/mL was the highest concentration tested for MA-non-AMP $IC_{50}$ and MIC values.